Ellerman Bombs, Type II White-light Flares and Magnetic Reconnection in the Solar Lower Atmosphere

Peng-Fei Chen⋆, Cheng Fang and Ming-De Ding

Department of Astronomy, Nanjing University, Nanjing 210093

Abstract   Ellerman bombs and Type II white-light flares share many common features despite the large energy gap between them. Both are considered to result from local heating in the solar lower atmosphere. This paper presents numerical simulations of magnetic reconnection occurring in such a deep atmosphere, with the aim to account for the common features of the two phenomena. Our numerical results manifest the following two typical characteristics of the assumed reconnection process: (1) magnetic reconnection saturates in ∼600–900 s, which is just the lifetime of the two phenomena; (2) ionization in the upper chromosphere consumes quite a large part of the energy released through reconnection, making the heating effect most significant in the lower chromosphere. The application of the reconnection model to the two phenomena is discussed in detail.

Key words: Sun: atmosphere—Sun: flares— Sun: magnetic fields

1   INTRODUCTION

Ellerman bombs (EBs), also known as moustaches, are small elongated brightening events which are observed in Hα wings around sunspots or under arch filament systems (AFS). They have a typical length of ∼1 arcsec (Kurokawa et al. 1982), and typical upward flow of ∼6 km s^{-1} in the chromosphere (Kitai 1983). EBs are cospatial with bright features in the 3840Å network, as well as with continuum facular granules (cf. Rust & Keil 1992), and are pushed away by expanding granules (Denker et al. 1995), where one polarity magnetic features may be driven to meet other opposite polarity features. It was suggested by many authors that the heating originates in the lower atmosphere (e.g., Kitai & Muller 1984; Dara et al. 1997). Recently, Ding, Hénoux, & Fang (1998) and Hénoux, Fang, & Ding (1998) reproduced typical EB line profiles by assuming that they are caused by nonthermal electrons preferentially originated in the lower chromosphere.

Solar white-light flares (WLFs) are among the strongest and rarest flaring events, with an increase in the visible continuum. They are of great importance in flare research because they are similar in many aspects to stellar flares, and because they present a major challenge to the

---

⋆ E-mail: chenpf@nju.edu.cn

flare atmospheric models and energy transport mechanisms (Neidig 1989). It was proposed that there are two types of WLFs which show distinctive emission features, i.e., Type I WLFs reveal a Balmer or Paschen jump, while Type II do not (Machado et al. 1986). Such a distinction results from different continuum radiation mechanisms: hydrogen free-bound transitions for Type I and negative hydrogen (H^-) radiation for Type II. Mauas, Machado, & Avrett (1990) are the first to investigate semi-empirical atmospheric models for WLFs, suggesting that white-light emission can appear in an active region with weak chromospheric emission and may correspond to heating of the lower layers in the atmosphere. Further systematic studies on both the spectral characteristics and atmospheric models for WLFs by Fang & Ding (1995) indicated that the features for Type I WLFs (e.g., a good time correlation between the emission of hard X-ray and the continuum, etc.) are well explained by the conventional flare picture: energy is initially released in the corona, then it is transported to the lower atmosphere and heats the plasma one after the other. However, for Type II, since the known mechanisms of energy transport are no longer effective (see Neidig 1989; Ding, Fang, & Yun 1999 for more references), an in situ heating mechanism deep in the chromosphere or the photosphere is required. Emslie & Machado (1979) and Mauas, Machado, & Avrett (1990) suggested that the required in situ heating may be due to local Joule dissipation of current. Recently, Li et al. (1997) proposed magnetic reconnection in a weakly ionized plasma as the in situ heating mechanism, by which they tried to account for some typical features of Type II WLFs: the length scale and the lifetime. However, their work is based on a linear analysis.

Magnetic reconnection is widely used to explain many coronal eruptive and/or heating events. Surges and some other chromospheric bursts are also thought to be induced by magnetic reconnection in a deep layer (e.g., Karpen, Antiochos, & Devore 1995). Indeed, more and more observational evidence is found for magnetic reconnection occurring in the lower atmosphere (e.g., Wang & Shi 1992). In this paper, 2D numerical simulations are performed to study the magnetic reconnection which occurs in the lower atmosphere, with the aim to account for some common features of EBs and Type II WLFs.

2   NUMERICAL METHOD

For magnetic reconnection in lower atmosphere, ionization and radiation become important, while heat conduction is negligible, contrary to the situation in the corona. In this partially ionized atmosphere, a multi-fluid model is sometimes applied to include the dissipation effect due to neutral-ion collisions. For simplicity, the weakly ionized plasma in this paper is approximately described by the one-fluid model, as was used in the hydrodynamics simulations by McClymont & Canfield (1983), which is justified when the coupling between ions and neutrals is very strong (Zweibel 1989). Another difficulty in 2D simulations of the lower atmosphere is the strong density stratification, since the pressure scale height is 100–600 km in the chromosphere/photosphere, resulting in a difference of about 7 orders of magnitude for the density between the top of the chromosphere and the lower photosphere. Incorporating such a stratification needs a very fine numerical mesh which makes the computations impractical. Thus, we further neglect the gravity and assume a uniform atmosphere by considering three cases with different characteristic densities.

The MHD equations are as follows:

$$\frac{\partial \rho}{\partial t} + \nabla \cdot (\rho \boldsymbol{v}) = 0, \tag{1}$$

$$\rho\frac{\partial \boldsymbol{v}}{\partial t} + \rho(\boldsymbol{v}\cdot\nabla)\boldsymbol{v} + \nabla P - \boldsymbol{j}\times\boldsymbol{B} = 0, \tag{2}$$

$$\frac{\partial \boldsymbol{B}}{\partial t} - \nabla\times(\boldsymbol{v}\times\boldsymbol{B}) + \nabla\times(\eta\nabla\times\boldsymbol{B}) = 0, \tag{3}$$

$$\frac{\partial}{\partial t}\left(\frac{P}{\gamma-1} + n_{\mathrm{e}}\chi_{\mathrm{H}} + \frac{\rho\boldsymbol{v}^2}{2}\right) + \nabla\cdot\left[\left(\frac{P}{\gamma-1} + n_{\mathrm{e}}\chi_{\mathrm{H}} + \frac{\rho\boldsymbol{v}^2}{2}\right)\boldsymbol{v}\right]$$
$$-\nabla\cdot(P\boldsymbol{v}) - \boldsymbol{E}\cdot\boldsymbol{j} + R - H = 0, \tag{4}$$

where $\nabla = \frac{\partial}{\partial x}\hat{\boldsymbol{e}}_x + \frac{\partial}{\partial y}\hat{\boldsymbol{e}}_y$, $\boldsymbol{v} = (v_x, v_y, v_z)$. The quantities ρ, $\boldsymbol{v}$, $\boldsymbol{B}$, and T have their usual meanings; $\boldsymbol{E}$ is the electric field, while $\boldsymbol{j}$ is the current density; R and H represent the radiative loss and the heating terms, respectively; the gas pressure $P = (n_{\mathrm{H}} + n_{\mathrm{e}})kT$, k is the Boltzmann constant, n_{H} and n_{e} are the number density of hydrogen atoms and electrons, respectively; χ_{H} is the ionization potential. n_{e} is deduced by a modified Saha and Boltzmann formula for pure hydrogen atmosphere:

$$n_{\mathrm{e}} = \begin{cases} (\sqrt{\phi^2 + 4n_{\mathrm{H}}\phi} - \phi)/2, & T \le 10^5\,\mathrm{K}, \\ n_{\mathrm{H}}, & T > 10^5\,\mathrm{K}, \end{cases} \tag{5}$$

where $\phi = \frac{1}{b_1}\left(\frac{2\pi m_{\mathrm{e}}kT}{h^2}\right)^{3/2}\mathrm{e}^{-\chi_{\mathrm{H}}/kT}$ (cf. Gan & Fang 1990). Radiation is important in the lower atmosphere. Strictly speaking, it should be solved by the non-LTE theory, which is too difficult to deal with in the present 2D simulations. Instead, it is substituted by an empirical formula given by Gan & Fang (1990):

$$R = n_{\mathrm{H}}n_{\mathrm{e}}\alpha(Z)f'(T), \tag{6}$$

where $\alpha(Z)$ and $f'(T)$ are functions of Z (the height from $\tau_{5000} = 1$ of the photosphere) and T (the temperature), respectively. Since gravity is neglected, α is set to be uniform accordingly, which is done by fixing the value of Z. The pre-heating rate is given by $H = n_{\mathrm{H}}\mathcal{H}$, where $\mathcal{H} = (n_{\mathrm{e}}\,\alpha f')_{t=0}$ is unchanged during the simulation.

In this paper, three cases (A, B, and C) are studied whose characteristic parameters (e.g., Z in Eq. (6), ρ_0 for the density, T_0 for the temperature, v_{A} for the velocity, t_{A} for the time, and β_0 for the ratio of gas to magnetic pressure) are shown in Table 1, where v_{A} is the Alfvén speed, $t_{\mathrm{A}} = L_0/v_{\mathrm{A}}$, and the length scale L_0 equals 2.5×10^8 cm in all cases. According to the canopy model, magnetic field decreases with increasing height Z. In our cases A, B, and C, the magnetic field is 12 G, 29 G, and 450 G, respectively. The parameters for cases A, B, and C correspond to conditions in the upper chromosphere, lower chromosphere, and photosphere, respectively. Hereafter, model A means case A without considering ionization and radiation, model AI means case A with ionization only, and model AIR means case A with both ionization and radiation considered. Similar notations are used for cases B and C.

Table 1 Models with Different Characteristic Parameters

Case	Z (10^5 cm)	ρ_0 (10^{-11} g cm^{-3})	T_0 (K)	v_{A} (10^5 cm s^{-1})	t_{A} (s)	β_0
A	1250	0.97	7800	16	158	1
B	625	16.7	5000	9	275	2
C	0	16700	5600	4.3	580	10

The domain of simulation is $-1 \le x/L_0 \le 1$, $0 \le y/L_0 \le 1$, along the horizontal x-axis and vertical y-axis, respectively; the initial static atmosphere is isothermal and uniform,

i.e., $\rho/\rho_0 = 1$ and $T/T_0 = 1$; the initial magnetic configuration is the same as in Chen et al. (1999a), i.e., a force-free current sheet. In this paper, an assumed anomalous resistivity $\eta/(\mu v_A L_0) = 0.01 \cos(5\pi x/L_0) \cos[10(y/L_0 - 0.5)\pi]$ is imposed in a local region $|x|/L_0 \le 0.1$, $|y/L_0 - 0.5| \le 0.05$ for cases A and B ($\eta = 0$ elsewhere). For case C, the resistivity region is shifted to $|x|/L_0 \le 0.1$, $|y/L_0 - 0.1| \le 0.05$. In the partially ionized atmosphere, the anomalous resistivity can be due either to molecular resistivity (Zweibel 1989), to the interaction between the ionized plasma and neutral gas (Cramer & Donnelly 1979), or to some other microscopic effects (e.g., the current driven instability), a detailed discussion of which is beyond the scope of this paper. Due to the symmetry about the y-axis, calculation is performed only in the right half region. The numerical mesh consists of 61×91 grid points, with 18 points lying within the half current sheet. Line-tying conditions are applied to the bottom boundary, and symmetry conditions to the left-hand side; other boundaries are free ones. The numerical simulations are performed with a multistep implicit scheme (Hu 1989). Also, an important numerical technique is applied to avoid possible pseudo-reconnection (cf. Chen, Fang, & Hu 2000).

3 NUMERICAL RESULTS

As anomalous resistivity sets in, two symmetrical convergent inflows move towards the diffusion region. Meanwhile, two narrow jets are ejected vertically. As indicated in our previous results (e.g., Chen et al. 1999a), the reconnected field lines above the reconnection point (X-point) are ejected along with the upward jet; their counterparts below the X-point, however, pile up due to the line-tying effect of the bottom boundary, so that the closed magnetic loop system rises. Figure 1 depicts the evolution of the temperature, velocity and magnetic configuration for model BIR. When the loop system gets close to the resistivity region, it hinders the reconnection inflow, and magnetic reconnection is slowed down. This saturation of magnetic reconnection was discovered by Chen et al. (1999b), who showed that the saturation time-scale is approximately proportional to the height of the X-point. Although the reconnection nearly stops after $t \sim 6\ \tau_A$, a global upward flow is seen, which results from the melon-seed effect of the magnetic configuration after the reconnection. The magnetic pressure gradient accelerates the plasma upward to a speed of $\sim 0.2v_A$. Similar evolution is found in other cases, only that
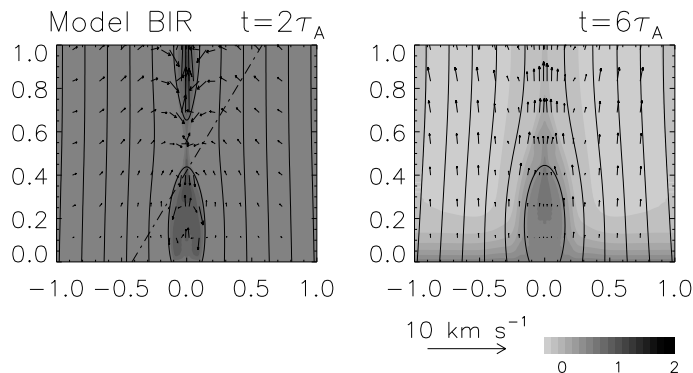

Fig. 1   Distributions of the temperature (grey scale), projected magnetic field (solid lines) and velocity field (vector arrows) in model BIR at two times ($t = 2\tau_A$ (left), $6\tau_A$ (right)).

in case A, the reconnection process is more violent due to its smaller β_0, whereas in case C, the reconnection is much slower. Since the magnetic energy in case C is much smaller than the thermal energy, the resulting heating is weak even in the model without ionization and radiation.

Figure 2 displays the time profile of the magnetic reconnection rate, R, defined as the closing rate of the field lines (Chen et al. 1999a). It can be seen that in any case the reconnection slows down self-consistently, with an e-folding decay time of $\sim$600–900 s, which is shown to be independent of the ionization and the radiation. It is also found that both ionization and radiation have very weak effect on the reconnection rate.
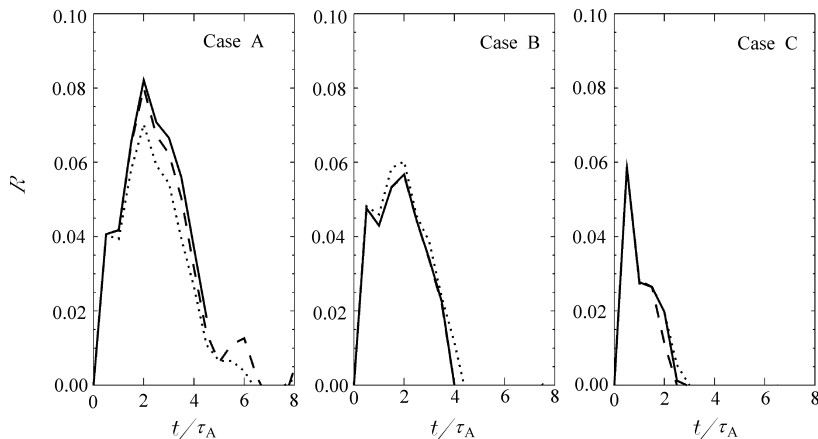

Fig. 2   Time profiles of magnetic reconnection rate (R) in the three cases. The unit of R is τ_A^{-1}. The dotted line corresponds to the model without ionization and radiation, the dashed line to the model with ionization only, and the solid line to the model with both ionization and radiation.

Compared to the energy release rate, the thermodynamic quantities (e.g., ρ T, etc.) are much more sensitive to the ionization and the radiation. The distributions of ρ and T in the three cases along the y-axis at $t = 400$ s are plotted in Figure 3. It can be seen that in case A, which characterizes the middle and upper chromosphere, the ionization process consumes a large part of the energy released through reconnection, and radiation further cools the plasma down so that the actual temperature increase ΔT is only 300 K at most, and $\sim$150 K in general with strong plasma condensation in the reconnection upflow; in case B, which characterizes the lower chromosphere, both the ionization and the radiation have a weak effect on T and ρ, resulting in a strong heating with ΔT up to $\sim$2000 K; in case C, which represents the photospheric level, a weak heating is produced even in the model without ionization and radiation with ΔT of $\sim$140 K.

4   DISCUSSION

Both the spectral observations and semi-empirical atmospheric models for EBs and Type II WLFs imply that an in situ heating mechanism in the chromosphere or photosphere may be

required to account for the Hα wing emission in EBs and continuum emission in WLFs (Kitai 1983; Fang & Ding 1995). Our numerical simulations of magnetic reconnection in the lower atmosphere show that both phenomena can be well explained by such a magnetic reconnection either from a dynamical or an energetic point of view.

(1) Saturation of the magnetic reconnection is self-consistently obtained in our simulations. As shown in Figure 2, the reconnection rate (R) falls down rapidly just after it rises to its maximum. This means that the low layer magnetic reconnection has a short lifetime. Judging from the e-fold decay time, the lifetime of such a reconnection is about 600–900 s in all models, which is consistent with that of EBs or WLFs.
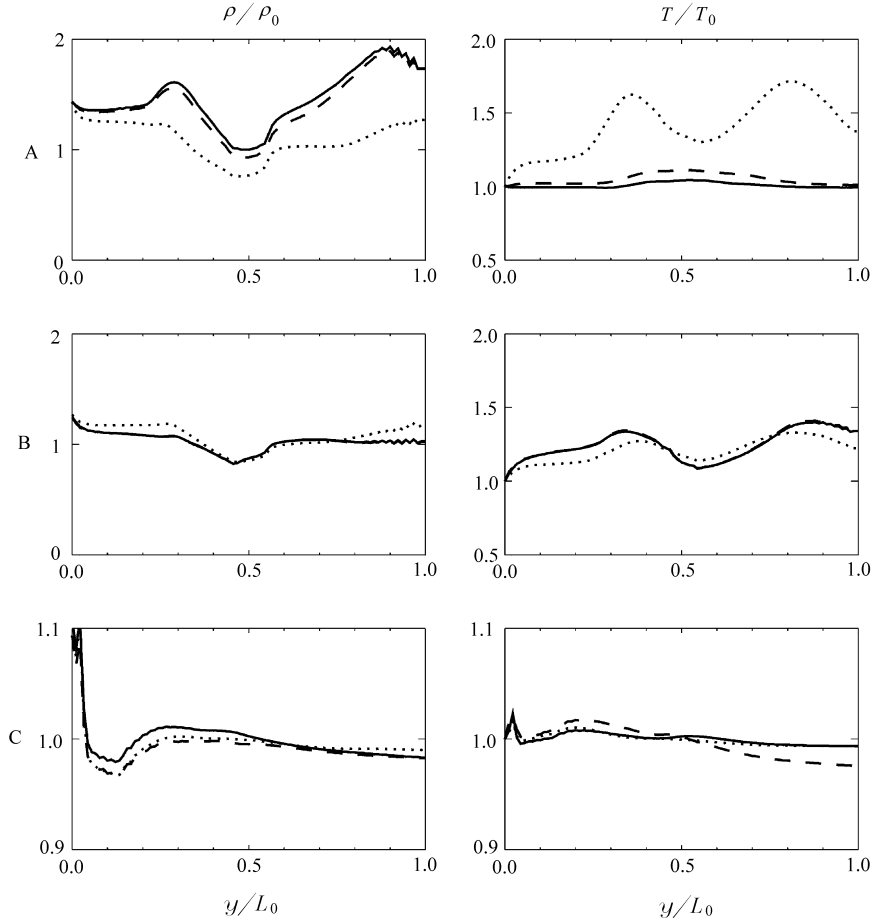

Fig. 3   Distributions of density and temperature in the three cases along the y-axis at $t = 400$ s. The dotted line corresponds to the model without ionization and radiation, the dashed line to the model with ionization only, and the solid line to the model with both ionization and radiation.

(2) The research by Zweibel (1989) shows that in the two-fluid model where the coupling between ions and neutrals is weak due to low ionization degree, reconnection proceeds more rapidly than that in the one-fluid model where the coupling is strong. Our results, on the

other hand, indicate that within the one-fluid frame, ionization process, as well as radiation process, has a very weak effect on the reconnection rate, and hence on the lifetime of magnetic reconnection.

(3) Numerical results indicate that in case A, most of the energy released by the reconnection in the upper chromosphere is converted into ionization potential, leading to a weak heating. On the contrary, the ionization in case B has a weak effect on T and ρ, resulting in a strong heating. This is due to the fact that the parameters in the upper chromosphere (case A) are in an ionization-sensitive regime, while those in case B are not. When T/T_0 increases from 1 to 1.7, the degree of ionization rises from 6% to 99% in case A, and only from 0.002% to 4% in case B. Kitai (1983) computed an atmospheric model for EBs, and found that the broad Hα wing is due to a formation of heated ($\Delta T = 1500$ K) and condensed plasma in the lower chromosphere. According to our models, localized magnetic reconnection leads to a temperature increase ΔT ~ 150–300 K in the upper chromosphere, and ~ 2000 K in the lower chromosphere (see Figure 3), which is in good agreement with Kitai's results.

In our model C, which represents the photosphere, the magnetic energy density is much smaller than the thermal energy density (i.e., high β), therefore, the release of magnetic energy results in weak heating, and ΔT in the bright region is only $\sim$140 K, as shown in Figure 3. However, this extra temperature increase in the flaring atmosphere is enough to account for the strong negative hydrogen ion (H$^-$) radiation (Fang et al. 1993), and is consistent with the atmospheric model for Type II WLFs (Fang & Ding 1995).

(4) Mass motions up to 6–8 km s^{-1} are found present in chromospheric layers of EBs (Kurokawa et al. 1982; Kitai 1983). Figure 1 shows an upflow with a speed of $\sim$ 6 km s^{-1}, which could possibly contribute to the observed blue asymmetry of the Hα line of EBs, although the blue asymmetry can not be simply interpreted as upward motion (Dara et al. 1997).
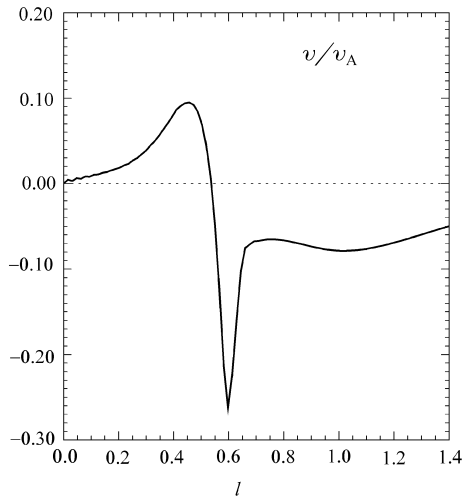
As regards Type II WLFs, observations indicate that the CaII K line presents a red asymmetry, i.e., the intensity at K_{1r} is stronger than that at K_{1b}, or, $I_r > I_b$ (Fang, Huang, & Hu 1985; Fang et al. 1986; Gan & Fang 1987). For the first time, Fang et al. (1992) systematically studied the red asymmetry of the CaII K line for 12 flares (including one Type II WLF). They showed that a downward mass motion above the temperature minimum region (TMR) can produce a red asymmetry of K_1. However, as they pointed out, if there exists only the downward motion, it would be difficult to reproduce quantitatively the observed value of $(I_r - I_b)/I_c$, especially for some large Type II WLFs, where I_c is the intensity of the related continuum. They suggested that an additional upward motion below TMR would help to increase the value of $(I_r - I_b)/I_c$. It implies that there is plasma contraction around the TMR. In the lower atmosphere reconnection scenario, the reconnection downflow

Fig. 4 Distribution of the line-of-sight velocity along the line $y/L_0 = x/L_0 + 0.42$. The velocity is scaled with v_A. Positive values mean an upward motion, while negative values a downward motion.

and the convergent inflow constitute the required contraction profile of velocity. To illustrate it, the line-of-sight velocity profile along the line $y/L_0 = x/L_0 + 0.42$ is plotted in Fig. 4. The line of sight is marked by a dotted line in Figure 1, where $l=0$ corresponds to its lower end, and $l=1.41$ to its upper end. It is interesting to find that the velocity profile is consistent with the contraction profile in figure 5 of Fang et al. (1992), i.e., the plasma in the upper part moves downward, while that in the lower part moves upward. Note that the symmetric inflows themselves can also produce the contraction velocity profile. However, it is very difficult for the velocity to reach the required values, 10–30 km s^{-1}, as proposed by Fang et al. (1992). The above analysis indicates that magnetic reconnection in the lower atmosphere can qualitatively explain some typical observational features of EBs and Type II WLFs. As future work, the construction of more accurate atmospheric models for EBs is important, and the relation between the magnetic reconnection in the low atmosphere and that in the corona is another thought-provoking problem.

5 CONCLUSIONS

Numerical simulations of magnetic reconnection in the solar lower atmosphere are performed in this paper. The main results can be summarized as follows:

1. Saturation is an intrinsic feature of magnetic reconnection due to the line-tying effect of the bottom boundary, which implies that the magnetic reconnection occurring in the lower atmosphere has a short lifetime. It is shown to be independent of the ionization and the radiation.

2. Both the ionization and the radiation have a weak effect on the magnetic reconnection

rate. However, they may alter the temperature and density distributions. Especially in the upper chromosphere, the thermal parameters are located in an ionization-sensitive regime, and ionization may consume quite a large part of the energy released by reconnection, leading to weak heating in the upper chromosphere. In the lower chromosphere, ionization and radiation have a weak effect on T and ρ, resulting in a localized strong heating.

3. Magnetic reconnection in the lower atmosphere can account for Ellerman Bombs and Type II WLFs in many observational aspects, such as the lifetime ($\sim$600 –900 s), the weak temperature rise in the upper chromosphere and in the photosphere ($\sim$150 K), and a strong heating in the lower chromosphere. Moreover, it can qualitatively provide the required upflow pattern above the reconnection point that explains at least part of the blue asymmetry of the EB line profiles, as well as the contraction velocity profile below the reconnection point that explains the observed red asymmetry of the Ca II K line in WLFs.

It is noted here that any WLF may be a mixture of both types (Types I and II) (Hiei 1982), and the present results may shed light on the transition region explosive events discovered by SOHO (Innes et al. 1997).

References

Chen P. F., Fang C., Tang Y. H., Ding M. D., 1999a, ApJ, 513, 516

Chen P. F., Fang C., Ding M. D., Tang Y. H., 1999b, ApJ, 520, 853

Chen P. F., Fang C., and Hu Y. Q., 2000, Chinese Science Bulletin, 45, 798

Cramer N. F., Donnelly I. J., 1979, PASAu, 3, 367

Dara H. C., Alissandrakis C. E., Zachariadis Th. G., Georgakilas A. A., 1997, A&A, 322, 653

Denker C., de Boer C. R., Volkmer R., Kneer F., 1995, A&A, 296, 567

Ding M. D., Fang C., Yun H. S., 1999, ApJ, 512, 454

Ding M. D., Hénoux J. -C., Fang C., 1998, A&A, 332, 761

Emslie A. G., Machado M. E., 1979, Solar Phys., 64, 129

Fang C., Ding M. D., 1995, A&AS, 110, 99

Fang C. et al., 1993, Sciences in China, Ser. A, 36, 217

Fang C., Gan W. Q., Huang Y. R., Hu J., 1986, In: The Lower Atmosphere of Solar Flares, D. F. Neidig ed., (Sunspot NM: NSO), 117

Fang C., Hiei E., Yin S. Y., Gan W. Q., 1992, PASJ, 44, 63

Fang C., Huang Y. R., Hu J., 1985, In: Proc. of Kunming Workshop on Solar Phys. and Interplanetary Travelling Phenomena, eds., C. de Jager, B. Chen, Beijing: Science Press, 765

Gan W. Q., Fang C., 1987, ApJ, 107, 311

Gan W. Q., Fang C., 1990, ApJ, 358, 328

Hénoux J. -C., Fang C., Ding M. D., 1998, A&A, 337, 294

Hiei E., 1982, Solar Phys., 80, 113

Hu Y. Q., 1989, J. Comput. Phys., 84, 441

Innes D. E., Inhester B., Axford W. I., Wilhelm K., 1997, Nature, 386, 811

Karpen J. T., Antiochos S. K., Devore C. R., 1995, ApJ, 450, 422

Kitai R., 1983, Solar Phys., 87, 135

Kitai R., Muller R., 1984, Solar Phys., 90, 303

Kurokawa H., Kawaguchi I., Funakoshi Y., Nakai Y., 1982, Solar Phys., 79, 77

Li X. Q., Song M. T., Hu F. M., Fang C., 1997, A&A, 320, 300

Machado M. E., Avrett E. H., Falciani R. et al., 1986, In: The Lower Atmosphere of Solar Flares, D. F. Neidig, ed., (Sunspot, NM: NSO), 483

Mauas P. J. D., Machado M. E., Avrett E. H., 1990, ApJ, 360, 715

McClymont A. N., Canfield R. C., 1983, ApJ, 265, 483

Neidig D. F., 1989, Solar Phys., 121, 261

Rust D. M., Keil L., 1992, Solar Phys., 140, 55

Wang J., Shi Z., 1992, Solar Phys., 140, 67

Zweibel E. G., 1989, ApJ, 340, 550